Microchimica Acta (2020) 187:155
https://doi.org/10.1007/s00604-020-4125-y

ORIGINAL PAPER

Electrochemiluminescence immunoassay for the prostate-specific antigen by using a CdS/chitosan/g-C_3N_4 nanocomposite

Bo Huang[1] · Xing-Pei Liu[1] · Jing-Shuai Chen[1] · Chang-jie Mao[1] · He-Lin Niu[1] · Bao-Kang Jin[1]

Received: 10 August 2019 / Accepted: 17 January 2020

Abstract

An electrochemiluminescence (ECL) biosensor was fabricated for the evaluation of prostate specific antigen (PSA). The sensor was developed by successively modifying glassy carbon electrode (GCE) electrodes with CdS/Chito/g-C_3N_4 nanocomposites and DNA1 was labeled at the 5′ end with thiol. The aptamer DNA was labeled at the 3′ end with a quencher ferrocene (Fc) was ligated to DNA1 by the principle of complementary base pairing. In the absence of PSA, the ECL intensity signal is effectively quenches through the energy transfer and photoexcitation electron transfer between CdS/Chito/g-C_3N_4 emitter and quencher Fc. After incubation with target PSA, the aptamer DNA interacts with PSA and then moved away from the electrode surface together, which will recover the ECL intensity. Under the optimal conditions, the ECL intensity increases linearly with the logarithm of PSA concentration in the range of 1 pg·mL^{-1} to 100 ng·mL^{-1}, and the detection limit is 0.14 pg·mL^{-1} (S/N = 3). The biosensor has been successfully applied to the determination of PSA in serum sample.

Keywords Biosensor · Quantum dots · Energy transfer · Ferrocene · Quenching · Serum · DNA

Introduction

Currently, prostate cancer has surpassed skin cancer to become the most common cancer in North American males [1–4]. Prostate specific antigen (PSA) and miRNA are typical biomarkers of prostate cancer. PSA is the most important early detection indicator of clinically significant prostate cancers [5–7]. Therefore, the early determination of PSA is particularly important. To date, various technical means have been proposed, such as enzyme-linked immunosorbent assay (ELISA) [8], photoelectrochemical (PEC) [9], fluorometric [10], and electrochemical [11]. However, great challenges still remain to find new approaches that could increase the sensitivity and selectivity of analytical methods at ultra-low concentrations in the earlier diagnosis of diseases. Therefore, there is a great need to develop a simple and highly sensitive method for determination of PSA.

✉ Chang-jie Mao
maochangjie@sina.com

[1] Anhui Province Key Laboratory of Chemistry for Inorganic/Organic Hybrid Functionalized Materials, School of Chemistry & Chemical Engineering, Anhui University, Hefei 230601, People's Republic of China

Electrochemiluminescence (ECL) analytical technique is widely favored by researchers because of its high sensitivity, low background signal, easy operation, and high controllability [12–17]. Compared with commonly used ECL illuminants (such as Ru(bpy)$_3^{2+}$, luminol), g-C_3N_4 is widely used as ECL sensor due to good thermal stability and non-toxic [18–20]. However, as the cathode potential increases, the ECL stability of g-C_3N_4 drops sharply, and electrode passivation may occur [21–24]. This limits the application of g-C_3N_4 to a certain extent. Therefore, it is necessary to improve the performance of g-C_3N_4. [25, 26]. As a commonly used semiconductor material, CdS has received extensive attention due to its excellent electrical, optical and electrochemical properties [27]. However, the electroluminescence stability of the pure CdS quantum dots in the aqueous reaction system is poor, so it is attempted to combine g-C_3N_4 with CdS. Due to the proper band gap and conduction band position, ECL strength and stability were found to be significantly improved compared to pure g-C_3N_4. Chitosan is a biopolymer rich in hydroxyl and amino groups with excellent permeability and affinity. In this study, it served as a stabilizer and binder between CdS and g-C_3N_4 nanocomposites, which was applied for establishing an ECL biosensor.

In this work, we proposed an ultra-sensitive ECL biosensor based on CdS/Chito /g-C_3N_4 composite material for effective

Published online: 05 February 2020

determination of PSA. CdS/Chito/C_3N_4 not only increases ECL strength and improves ECL stability, but also indirectly provides a binding point for PSA aptamers. As shown in Scheme 1, the CdS/Chito/g-C_3N_4 nanocomposite was firstly added to the surface of the glassy carbon electrode, and then DNA1 was attached to the electrode through the Cd-S bond, followed by the dropwise addition of mercaptoethanol (MCH) to block the excess active site. Subsequent to the principle of complementary pairing, the quencher ferrocene (Fc)-labeled DNA2 was modified onto the electrode, resulting in quenching of the ECL signal by energy transfer and photoexcitation electron transfer [26, 28–30]. When the target PSA is present, DNA2 specifically binds to the target PSA, and then together with the electrode surface, the ECL signal will significantly recover. The sensor can detect PSA with high sensitivity and high selectivity, and is expected to be used for clinical diagnosis.

Experimental section

Materials

Prostate specific antigen (PSA) was synthesized by Shanghai Sangon Biotechnology Co. (Shanghai, China, www.sangon.com). 3-mercaptopropionic acid (MPA), thioacetamide (TAA) were bought Macklin Biochemical Co. Ltd. (Shanghai, China, www.macklin.cn). Cadmium ($CdCl_2$), chitosan (CS) were obtained from Aladdin Industrial Company (Shanghai, China, www.aladdin-e.com), sodium phosphate monobasic dihydrate ($NaH_2PO_4 \cdot 2H_2O$), Potassium phosphate monobasic (Na_2HPO_4), Potassium ferrocyanide trihydrat ($K_4Fe(CN)_6 \cdot 3H_2O$), potassium ferricyanide ($K_3Fe(CN)_6$) was purchased from Tianjin Guangfu Technology Development Co., Ltd. (Tianjin, China, www.guangfubiaowu.com). Glacial acetic acid (HAC), potassium

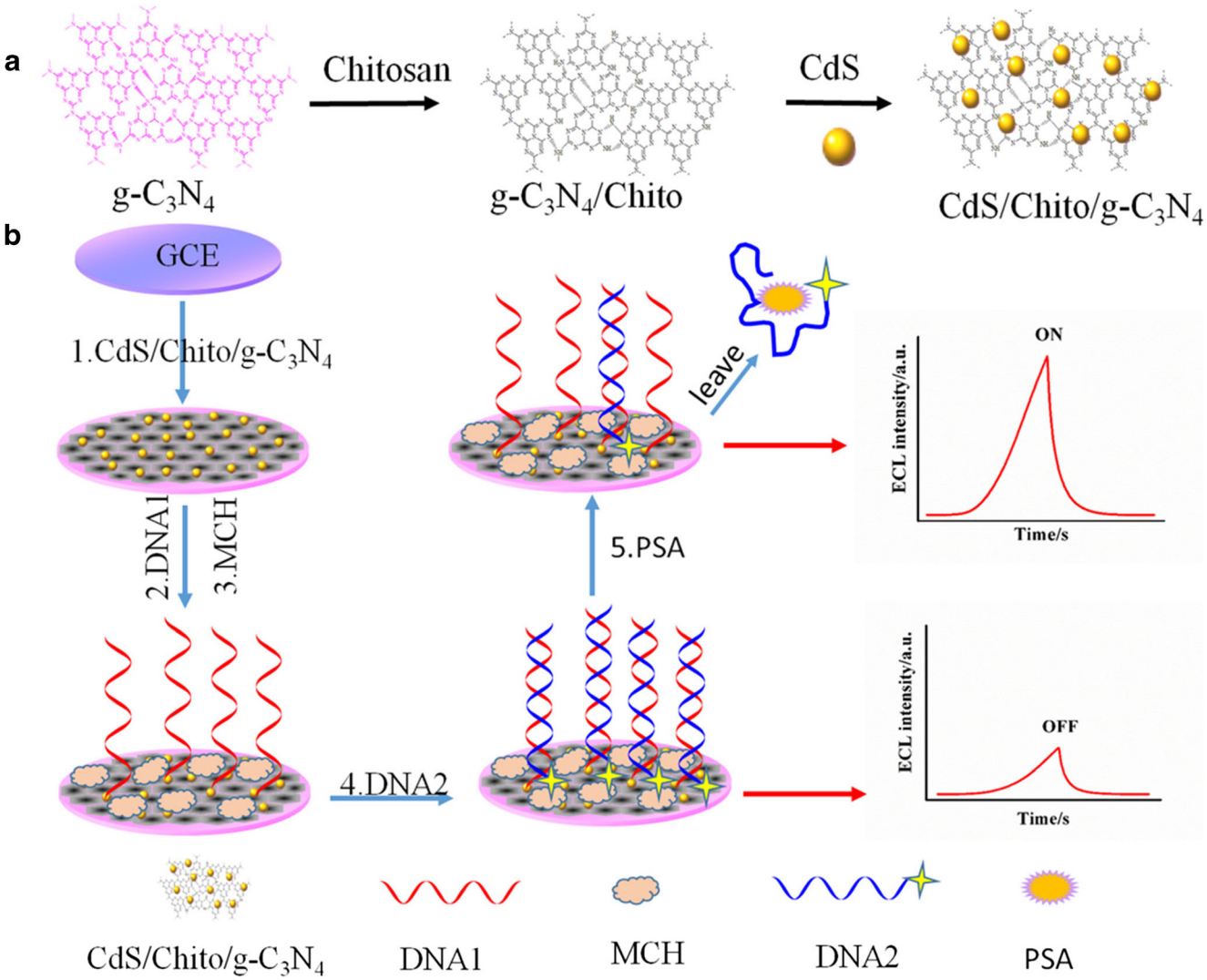

Scheme 1 Schematic diagram of an ultrasensitive biosensor for detection of PSA

chloride (KCl), potassium persulfate were bought from Sinopharm Group (Shanghai, China, www.sinopharmholding.com). Melamine ($C_3H_6N_6$), Tris-(2-carboxyethyl)-phosohine hydrochloride (TCEP), TE buffer, were bought Shanghai Sangon Biotechnology Co. (Shanghai, China, www.sangon.com). Sodium chloride (NaCl), sodium hydroxide (NaOH) were purchased Tianjin Damao Chemical Reagent Factory (Tianjin, China, www.dmreagent.com). 6-mercaptohexan-1-ol (MCH) was obtained Saan Chemical Technology (Shanghai) Co., Ltd.(Shanghai, China, www.energy-chemical.com).

DNA was synthesized by Shanghai Sangon Biotechnology Co.
DNA sequence was as follows:
DNA1: 5'-SH-$(CH_2)_6$-GCTATTTGATGGCGAGCTTTAAT-3'.
DNA2(Fc-DNA): 5'-ATTAAAGCTCGCCATCAAATAGC-$(CH_2)_6$-Fc-3'.

The DNA solution was set to the appropriate concentration with TE buffer solution, and PSA was diluted to varying concentrations with phosphate-buffered saline (PBS) (pH 7.4).

Apparatus

Electrochemical measurement and ECL signal measurement were performed using a CHI 650D (Chenhua, Shanghai, China, www.chinstr.com) and RFL-1 ultra-weak chemiluminescence/bioluminescence detector (Remax, Xi'an, China, www.chinaremex.com). Electrochemical impedance spectroscopy (EIS) was recorded using a CIMPS photoelectrochemical comprehensive test instrument (Zahner, Germany, www.zahner.com), with a three-electrode system: a platinum wire electrode, which acts as a counter electrode, Ag/AgCl as the reference electrode, and glassy carbon electrode (GCE, $\Phi = 4$ mm) as the working electrode. JEM-2100 transmission electron microcopy (JEOL, Japan, www.instrument.com), UV-3600 UV-Vis absorption spectroscopy (Shimadzu, Japan, www.esugimoto.com), and X-ray powder diffractions (XRDs) were performed on an D/max-rA X-ray diffractometer (Rigaku, Japan, www.rigaku.com).

Synthesis of CdS/Chito/g-C_3N_4 nanocomposites

The g-C_3N_4 was synthesized according to the method described in the literature with slight modifications [25, 26]. Briefly, 2 g of melamine was placed into the muffle furnace for calcination at 550 °C for 4 h at a heating rate of 3 °C·min^{-1}. After cooling to room temperature, the obtained bulk was milled into powder and then furtherly heated at 500 °C for 2 h at a heating rate of 5 °C·min^{-1}. The resultant powder was redispersed in ultrapure water with a concentration of 1 mg/mL and continuously ultrasonicated for 12 h. The upper suspension was sonicated at 6000 rpm for 10 min. The resultant supernatant was collected and stored at 4 °C. The g-C_3N_4 supernatant was mixed firstly with a 0.5 wt% of chitosan solution for 30 min, then centrifuged several times with deionized water. The precipitate was dispersed with deionized water to form 1 mg·mL^{-1} solution.

The CdS quantum dots were synthesized as previously reported [31]. 172 μL of Mercaptopropionic acid (MPA) was added to 40 mL of 20 mM $CdCl_2$ solution. NaOH (1 M) was added to adjust the pH value to 11, then pure N_2 bubbled through for 30 min to remove O_2. Thioacetic acid (TAA; 40 mL of 20 mM) was then poured into a three-necked flask and heated in an oil bath at 80 °C. After 2 h of continuous operation, the reaction liquid was removed and cooled naturally. Ethanol was added the above solution and then was centrifuged at 6000 rpm for 10 min. The precipitate was redispersed in the 8 mL of deionized water.

To prepare CdS/Chito/g-C_3N_4 nanocomposites solution, 1 mg·mL^{-1} g-C_3N_4/Chito solution was mixed with 0.01 M CdS QDs solution with the volume ratio of 1:3 by mild sonication for 30 min.

Fabrication of the electrochemiluminescence DNA sensor and the measurement procedure

Prior to fabrication, the GCE was carefully polished with 0.3 μM R-Al_2O_3 powder and washed ultrasonically with deionized water and dried with nitrogen. As shown in Schemes 1, 10 μL of CdS/Chito/g-C_3N_4 suspensions were dropped onto the pretreated GCE and dried at room temperature. Next, DNA1 (15 μL) was dropped onto the electrode surface. Following incubation at room temperature, 10 μL of 6-mercaptohexanol (MCH) solution was dropped (overnight at 37 °C) to block the non-specific active binding sites. The electrode was then coated with 15 μL of Fc-DNA at 37 °C for 1.5 h. Finally, the GCE|CdS/Chito/g-C_3N_4|DNA1|MCH|Fc-DNA modified electrode was incubated in 15 μL of the varying target PSA concentration samples at 37 °C. The electrode was washed thoroughly with deionized water to remove superfluous reagents and dried with nitrogen after each step of the incubation process.

Electrochemiluminescence determination

ECL measurements were carried out in 5 mL of 0.1 mol·L^{-1} PBS (pH 7.4) containing 0.1 mol·L^{-1} of $K_2S_2O_8$ and 2.7 mol·L^{-1} of KCl with the photomultiplier tube voltage setting at 400 V. The working potential was from −1.45 V to 0 V at a scan rate of 0.1 V/S.

Results and discussion

Characterization of CdS/Chito/g-C_3N_4 nanocomposites

Figure 1 shows the XRD peaks of CdS, g-C_3N_4 and CdS/Chito/g-C_3N_4 nanocomposite, respectively. The CdS quantum dots showed peaks at 2θ = 52.1°, 43.9° and 26.5°, matching the crystal faces of (311), (220) and (111) (PDF#10–0454) [32]. The 2D g-C_3N_4 nanostructure had two characteristic peaks at 27.4° and 13.2°, corresponding to (002) and (100) diffraction planes. For the CdS/Chito/g-C_3N_4 nanocomposites, a characteristic diffraction peak of CdS at (111) was detected, and the others were uniformly paired. This preliminary test confirmed that CdS/Chito/g-C_3N_4 nanocomposites was fabricated successfully.

Figure 2 shows the microstructure and morphology of g-C_3N_4 and CdS/Chito/g-C_3N_4. As shown in Fig. 2a, pure g-C_3N_4 was successfully stripped from large fragments, clearly showing the thin layered structure of g-C_3N_4. Figure 2b shows that CdS is evenly distribute on the surface of g-C_3N_4, indicating that CdS is tightly immobilized on the surface. Figure 2c is a high-resolution transmission electron micrograph (HRTEM) of CdS/Chito/g-C_3N_4, which clearly shows the lattice fringes of CdS quantum dots. The average particle size is ~2.5 nm, corresponding to the (111) crystal plane of CdS [32, 33]. Energy dispersive spectroscopy (EDS) was used to evaluate the chemical composition of the nanocomposite CdS/Chito/g-C_3N_4. As shown in Fig. 2d, peaks corresponding to the C, N, Cd, and S elements were observed. The other peak originates from the substrate of the sample disk.

Figure 2e shows the UV-Vis absorption spectra of CdS, g-C_3N_4 and CdS/Chito/g-C_3N_4, respectively. It shows that the maximum absorption peak of the CdS quantum dots was ~380 nm, and g-C_3N_4 has a characteristic absorption peak at 328 nm, which is consistent with the previous report [31]. The figure shows that the two absorption peaks of CdS/Chito/g-C_3N_4 coincide with the absorption peaks of CdS quantum dots and g-C_3N_4, respectively, which proves that the CdS quantum dots have been successfully supported on the surface of g-C_3N_4.

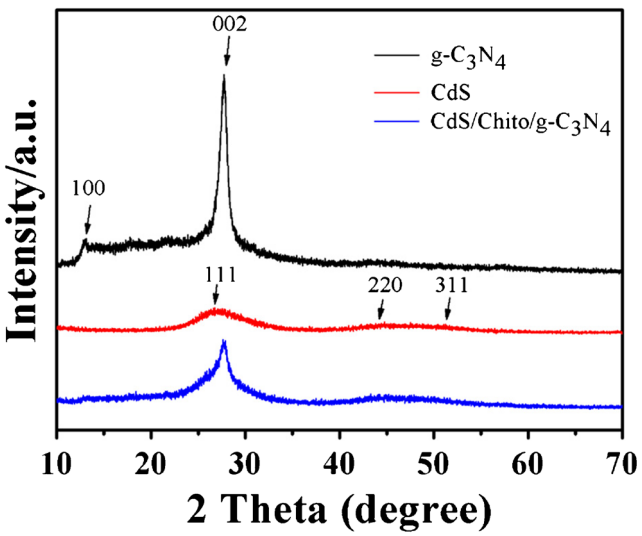

Fig. 1 XRD patterns of g-C_3N_4, CdS and CdS/Chito/g-C_3N_4

Electrochemiluminescence behavior and mechanism

Based on the CdS/Chito/g-C_3N_4 sensor for detecting PSA, chitosan is favored because of its good adhesion and biocompatibility, DNA1 is attached to the surface of GCE by Cd-S bond. DNA1 is treated with TCEP before addition, and the disulfide bond is broken while forcing the modified DNA1 to be in vertical contact. The MCH solution is added to block non-specific active binding sites on the electrode surface, and then combined with the Fc-attached DNA2 by the principle of complementary base pairing. The introduction of ferrocene aptamer DNA was achieved by energy transfer and optometry. Electron transfer can effectively quench the ECL signal, that is, the excited CdS/Chito/g-C_3N_4* energy is transferred to the Fc. When the target PSA is present, the aptamer DNA binds to the target, i.e., it leaves the electrode surface, and the ECL signal is recovered due to the adaptation. The binding force between the bulk DNA and the target is stronger than the hydrogen bond strength between the double-stranded complements. Otherwise, the ECL signal is annihilated. According to previous studies [34], the ECL mechanism of CdS/Chito/g-C_3N_4 may be as follows:

$$\mathrm{CdS/Chito/g{-}C_3N_4} + \mathrm{e^-} \rightarrow \mathrm{CdS/Chito/g{-}C_3N_4^{\bullet -}} \quad (1)$$

$$\mathrm{S_2O_8^{2-}} + \mathrm{e^-} \rightarrow \mathrm{SO_4^{\bullet -}} + \mathrm{SO_4^{2-}} \quad (2)$$

$$\mathrm{CdS/Chito/g{-}C_3N_4^{\bullet -}} + \mathrm{SO_4^{\bullet -}} \rightarrow \mathrm{CdS/Chito/g{-}C_3N_4^{*}} + \mathrm{SO_4^{2-}} \quad (3)$$

$$\mathrm{CdS/Chito/g{-}C_3N_4^{*}} \rightarrow \mathrm{CdS/Chito/g{-}C_3N_4} + h\nu \quad (4)$$

During the negative potential scanning, CdS/Chito/g-C_3N_4 is reduced to CdS/Chito/g-$C_3N_4^{\bullet -}$ (Eq. (1)), and the co-reactant $S_2O_8^{2-}$ is reduced to strong oxidant $SO_4^{\bullet -}$ (Eq. (2)). Then CdS/Chito/g-$C_3N_4^{\bullet -}$ can be excited by $SO_4^{\bullet -}$ to form excited state CdS/Chito/g-$C_3N_4^{*}$ (Eq. (3)). CdS/Chito/g-$C_3N_4^{*}$ is very unstable, easily loses electronic transition to ground state, and produces ECL luminescence (Eq. (4)).

Characteristics of the sensor construction process

To verify the successful assembly of the sensor layer, we carried out cyclic voltammetry (CV) and EIS tests. As shown in Fig. 2f, the bare electrode (curve a) showed a good redox peak current. When the CdS/Chito/g-C_3N_4 nanocomposite (curve

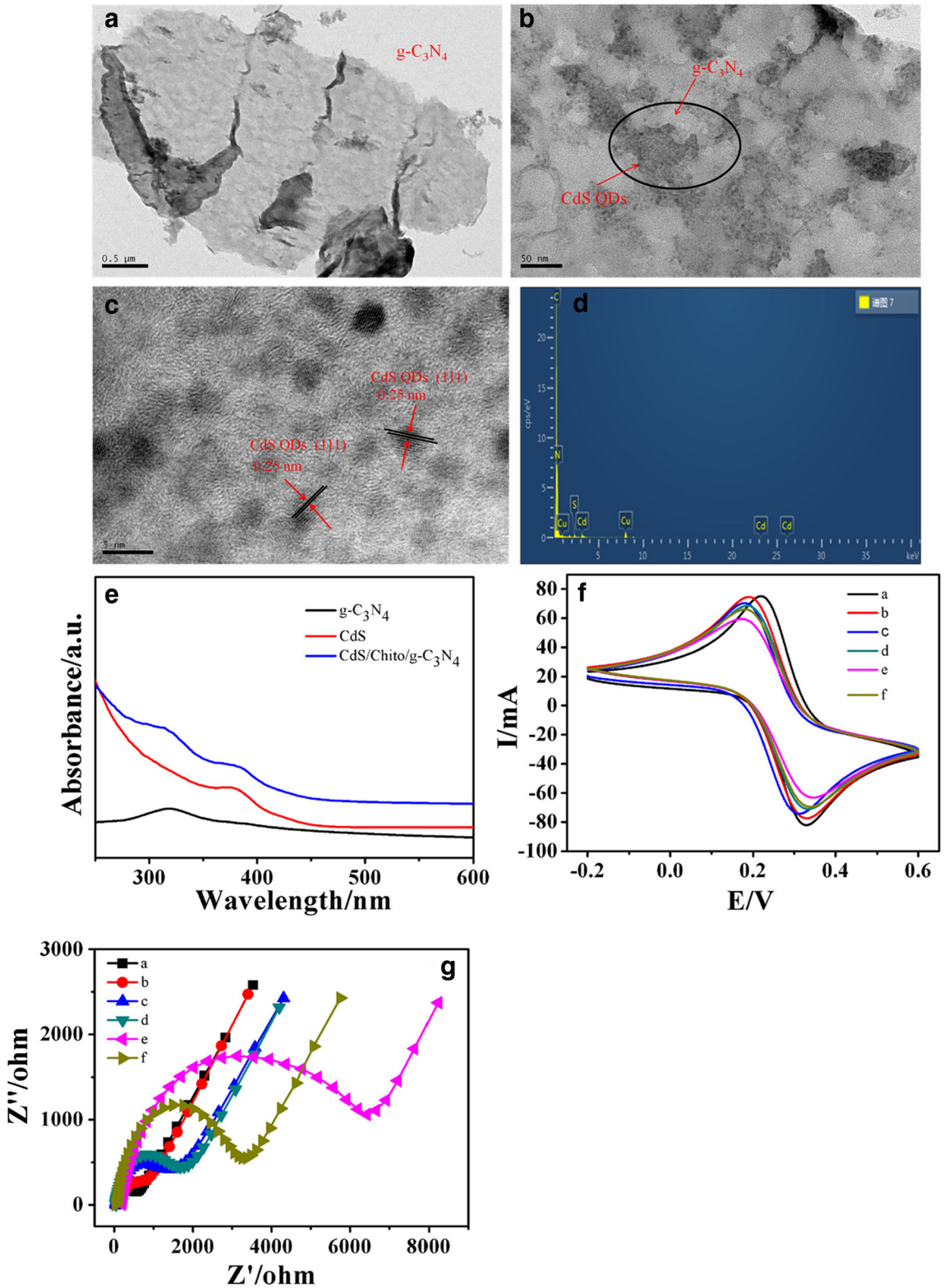

Fig. 2 TEM image of **a** g-C_3N_4 and **b** CdS/Chito/g-C_3N_4. **c** HRTEM image of CdS/Chito/g-C_3N_4. **d** EDS spectra of the CdS/Chito/g-C_3N_4. **e** UV-Vis absorption spectra of g-C_3N_4, CdS and CdS/Chito/g-C_3N_4. **f** The curves of cyclic voltammetry and **g** EIS for the stepwise biosensor fabrication measured in 2.0 mM $[Fe(CN)_6]^{3-/4-}$ containing 0.1 M KCl, with the scan range of −0.2 to 0.6 V and rate of 100 mV/s. (a) bare GCE. (b) CdS/Chito/g-C_3N_4. (c) GCE|CdS/Chito/g-C_3N_4/DNA1. (d) GCE|CdS/Chito/g-C_3N_4/DNA1|MCH. (e) GCE|CdS/Chito/g-C_3N_4/DNA1|MCH|DNA2. (f) GCE|CdS/Chito/g-C_3N_4/DNA1|MCH|DNA2|PSA

b) was coated onto the surface of the electrode, the peak current was remarkably lowered, and the electron transfer rate slowed. As the DNA1 (curve c), MCH (curve d), and DNA2 (curve e) layers were assembled onto the surface of the modified electrode, the peak current gradually decreased. This was mainly due to the fact that the non-conductive substance modified on the surface of the electrode greatly reduced the electron transfer process. When the target antigen PSA (curve f) was continuously added and incubated on the electrode surface, the PSA specifically bound to the DNA2 and left the electrode surface altogether, such that the redox peak current of the modified electrode increased. Thus, the above results indicate that the layer assembly of the sensor was successful.

In order to better understand the layer assembly process of the modified electrode, Fig. 2g shows the EIS spectra of different modified electrodes. The bare electrode showed a relatively small electron transfer resistance (Ret) (curve a). When CdS/Chito/g-C_3N_4 was modified to the surface of the GCE, the Ret value was larger than that of the bare electrode (curve b), showing that CdS/Chito/g-C_3N_4 can block the electrons on $[Fe(CN)_6]^{3-/4-}$ on the electrode surface. As DNA1, MCH and DNA2 were successively modified on the surface of the electrode prepared above, the Ret value was further increased (curves c, d and e), and when the target PSA was added, DNA2 specifically binds to the target PSA and then leaves the electrode surface together, the Ret had slightly decreased (curve f). These EIS results are consistent with what was expected, indicating that the proposed ECL biosensor had been successfully constructed.

Optimization of the experimental conditions

In order to obtain a strong and stable ECL signal, the optimization experiments with different volume ratios of Chito/g-C_3N_4 and CdS were studied. When the volume ratio of Chito/g-C_3N_4 to CdS is 3: 1, the nanocomposite has the largest ECL intensity (Fig. 3a). To control the variables, the DNA1

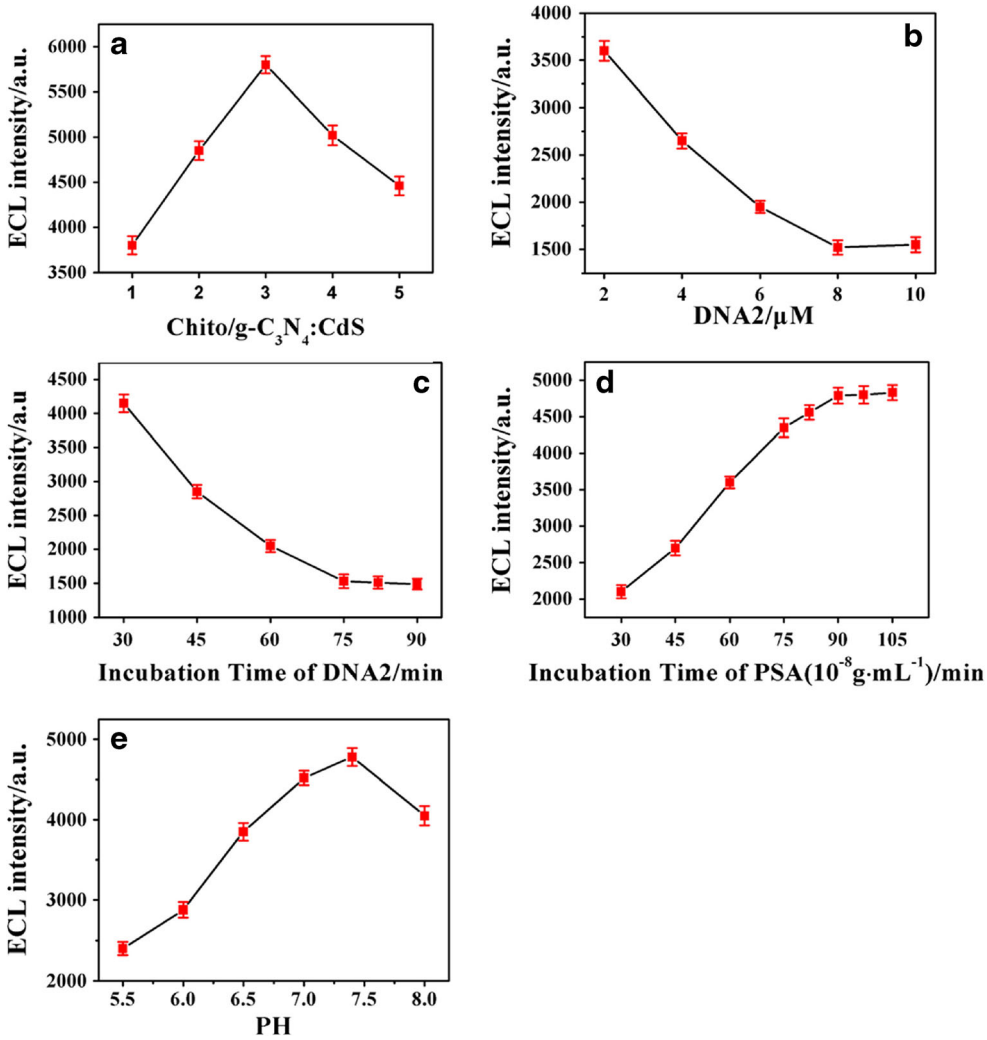

Fig. 3 Influence of **a** the value of volume ratio between Chito/g-C_3N_4 and CdS, **b** concentration of DNA2, **c** incubation time with DNA2, **d** incubation time with PSA, **e** the PH value

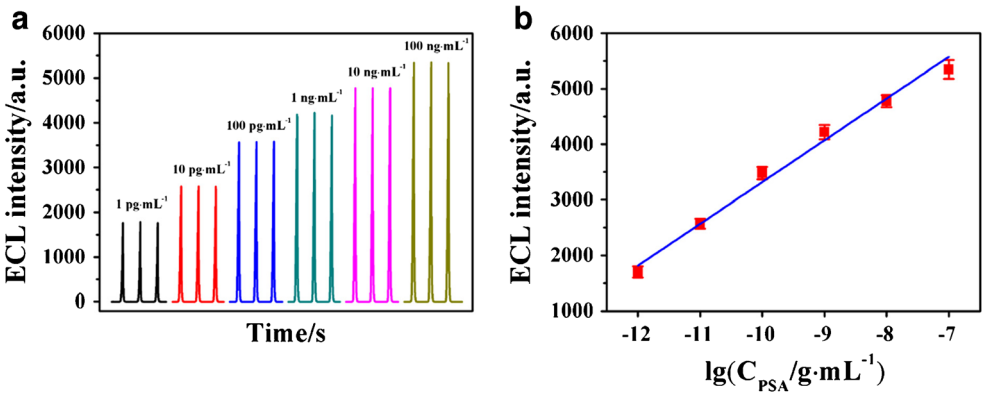

Fig. 4 **a** ECL response of the designed biosensor in the presence of different PSA concentrations. **b** Calibration plot of the biosensor for the target PSA at different concentrations

concentration was determined as 2 μM. The optimal DNA2 concentration, the optimal DNA2/DNA1 incubation time, and incubation time of PSA with sensors directly affect sensor performance. Figure 3b shows that when the DNA1 concentration was 2 μM, the ECL intensity decreased with increasing DNA2 concentration. As the DNA2 concentration increased to 8 μM, the ECL intensity was the lowest, i.e., the quenching was optimal, and the DNA2 concentration continued to increase. The ECL intensity had a tendency to increase slowly. Therefore, 8 μM was used as the optimal DNA2 concentration in the following experiment. Figure 3c shows that when determining the optimal DNA2 concentration, as the incubation time of DNA2 and DNA1 increases, the ECL intensity gradually decreases, and then there is almost no significant change after 75 min. Therefore, the optimal incubation time for this experiment is 75 min. From Fig. 3d, we can see that as the incubation time of the PSA and the sensor increases, the ECL intensity gradually increased, and then ECL signal had no longer any obvious change at 90 min. Therefore, the optimal incubation time was 90 min for the entire experiment. In addition, the pH value also affect the performance of the sensor. Figure 3e shows that the ECL signal increases firstly and then decreases as the pH value increases. When the pH value is 7.4, the ECL intensity reaches a maximum value. This phenomenon indicates that more negatively charged substances could promote electron transfer. When the pH value is higher than 7.4, excess anions are accumulate on the electrode surface, thereby inhibiting the approach of the negatively charged CdS quantum dots, resulting in a decrease in ECL intensity. Therefore, the pH value of 7.4 is the best experimental condition.

Performance study of the sensor

After determining the optimal conditions, the sensor performance was evaluated by detecting the ECL intensity at a range of different PSA concentrations. Figure 4a shows that as the PSA concentration increases, the ECL intensity gradually increases. The reason for this phenomenon is that the aptamer DNA2 binds to the target PSA, and is detached from the electrode surface, thereby restoring the ECL intensity. Additionally, the ECL intensity change was linear with the PSA concentration logarithm. Figure 4b shows the sensor versus PSA determination standard plot. The linear range of determination was 1 pg·mL^{-1} to 100 ng·mL^{-1}, and the linear equation was $I = 10{,}846.3 + 752.8lgC$ (g·mL^{-1}). The correlation coefficient was R = 0.994, and the detection limit was 1.4×10^{-13} g·mL^{-1} (S/N = 3). Compared with the previous report about determination of PSA (As shown in Table 1), the sensor showed a relatively low detection limit and the wide linear range.

Adaptability, stability and selectivity of the sensor

To evaluate the repeatability of the sensor, six electrodes were incubated under the same conditions at the same

Table 1 In contrast to other previously reported PSA immunosensors

Analytical method	Electrode materials	Linear range	Limit of detection	Reference
PEC	Mn:CdS /g-C_3N_4	0.01 ng·mL^{-1}-20 ng·mL^{-1}	3.8 pg·mL^{-1}	[20]
ECL	CdS–Au	1 ng·mL^{-1}-12 ng·mL^{-1}	0.6 ng·mL^{-1}	[27]
Fluorescence	Ag@SiO_2@SiO_2-RuBpy	0.1 ng·mL^{-1}-100 ng·mL^{-1}	27 pg·mL^{-1}	[10]
ELISA	—	0.825 ng·mL^{-1}-165 ng·mL^{-1}	0.16 ng·mL^{-1}	[8]
ECL	CdS/Chito/g-C_3N_4	1 pg·mL^{-1}-100 ng·mL^{-1}	0.14 pg·mL^{-1}	This work

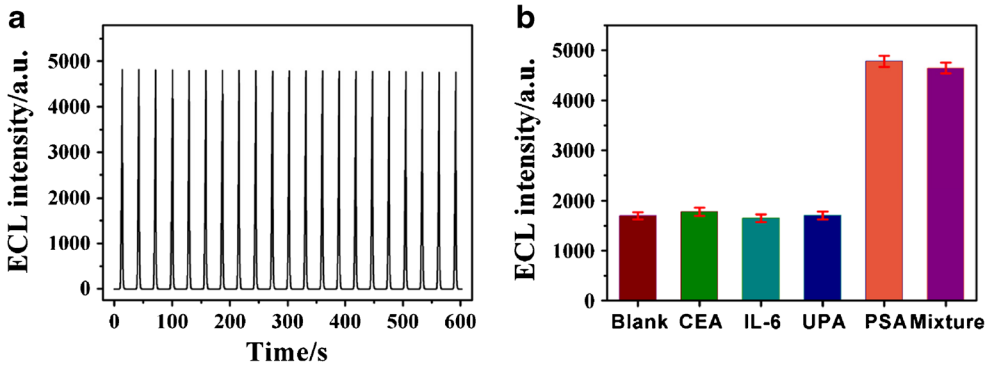

Fig. 5 **a** The ECL stability of the aptasensor with the concentration of PSA (10 ng/mL) under a continuous cyclic potential scan for 20 cycles. **b** The selectivity of the proposed ECL aptasensor detection of PSA (10 ng·mL^{-1}) against different targets: CEA (10 μg·mL^{-1}), IL-6 (10 μg·mL^{-1}), UPA (10 μg·mL^{-1}) and a mixture (10 ng·mL^{-1} PSA, 10 μg·mL^{-1} CEA, 10 μg·mL^{-1} IL-6, 10 μg·mL^{-1} UPA). Error bars: SD, $n = 3$

concentration, and the ECL intensity values were compared. The relative standard deviation of the sensor was 2.42%, indicating fairly good repeatability.

To test the stability of the constructed sensor, we carried out a continuous scan of the incubated electrode for 20 cycles, showing satisfactory results (Fig. 5a). The incubated electrode was then stored at 0–4 °C. After 2 weeks of removal, the measured ECL intensity increased by 4.6% compared with the previous one, without much change, showing good storage stability.

To evaluate the response of the designed immunosensor to other interfering substances, we studied urokinase-type plasminogen activator (UPA, 10 μg·mL^{-1}), carcinoembryonic antigen (CEA, 10 μg·mL^{-1}) and interleukin-6. (IL-6, 10 μg·mL^{-1}) was used as interference detection for the sensor. As a result, as shown in Fig. 5b, it is not difficult to find that the ECL intensity change of the sensor is negligible compared with the blank. However, when the sensor was incubated with 10 ng·mL^{-1} PSA and 10 μg·mL^{-1} of a mixture of the above various interfering substances, there was no significant change in the ECL intensity of the sensor compared to incubation with only PSA. The above results indicate that the sensor shows better selectivity.

Table 2 Detection of PSA in human serum samples

Serum samples	PSA hospital (ng·mL^{-1})	This work (ng·mL^{-1})	Relative deviation (%)
1	14.40	14.88	3.06
2	9.42	9.81	4.14
3	8.38	8.13	−2.98
4	5.56	5.27	−5.22
5	0.42	0.44	4.76
6	0.094	0.098	4.26

Human serum sample analysis

In order to verify the feasibility and accuracy of the designed biosensor, the sensor was used to detect real human serum samples. Compared with the results of the First Affiliated Hospital of Anhui Medical University (Chemiluminescence Immunoassay), the results are shown in Table 2. It can be seen that the designed ECL biosensor maintains good consistency with the hospital test results, indicating that the sensor has potential application value in clinical diagnosis in the future.

Conclusions

This work has proven that ECL immunization biosensor can detect PSA efficiently and sensitively. Based on the presence of CdS/Chito/g-C_3N_4 nanocomposites, the sensor exhibits a fairly strong and stable ECL signal. The sensor has the advantages of wide linear range, high sensitivity and easy operation. This method is expected to have great potential in the application in the clinical diagnosis of PSA.

Acknowledgments This work was supported by the National Natural Science Foundation of China (Grant Nos. 21575001, 21976001), Natural Science Foundation of Anhui Province (1808085QB53). Open fund for Discipline Construction of Institute of Physical Science and Information Technology.

Compliance with ethical standards

Conflict of interest The author(s) declare that they have no competing interest.

References

1. Kostova MB, Rosen DM, Chen Y, Mease RC, Denmeade SR (2013) Structural optimization, biological evaluation, and

application of peptidomimetic prostate specific antigen inhibitors. J Med Chem 56:4224–4235
2. Ma Y, Shen XL, Zeng Q, Wang LS (2017) A glassy carbon electrode modified with graphene nanoplatelets, gold nanoparticles and chitosan, and coated with a molecularly imprinted polymer for highly sensitive determination of prostate specific antigen. Microchim Acta 184:4469–4476
3. Pérez-Ibave DC, Burciaga-Flores CH, Elizondo-Riojas MÁ (2018) Prostate-specific antigen (PSA) as a possible biomarker in non-prostatic cancer: a review, Cancer. Epidemiol 54:48–55
4. Feng Z, Zhi ST, Guo L, Zhou Y, Lei C (2019) An integrated magnetic microfluidic chipfor rapid immunodection of the prostate specific antigen using immunomagnetic beads. Microchim Acta 186: 252
5. He Y, Xie SB, Yang X, Yuan R, Chai YQ (2015) Electrochemical peptide biosensor based on in situ silver deposition for detection of prostate specific antigen. Acs Appl Mater Inter 7:13360–13366
6. Jemal A, Bray F, Center MM, Ferlay J, Ward E, Forman D (1900) Global cancer statistics. CA- Cancer J Clin 61:69–90
7. Fang QC, Lin ZH, Lu FS, Chen YW, Huang XC, Gao WH (2019) A sensitive electrochemiluminescence immunosensor for the detection of PSA based on CdWS nanocrystals and Ag+@UIO-66-NH_2 as a novel coreaction accelerator. Electrochim Acta 302:207–215
8. Lang QL, Wang F, Yin L, Liu MJ, Petrenko VA, Liu AH (2014) Specific probe selection from landscape phage display library and its application in enzyme-linked immunosorbent assay of free prostate-specific antigen. Anal Chem 86:2767–2774
9. Zhou Q, Lin YX, Zhang KY, Li MJ, Tang DP (2017) Reduced graphene oxide/$BiFeO_3$ nanohybrids-based signal-on photoelectrochemical sensing system for prostate-specific antigen detection coupling with magnetic microfluidic device. Biosens Bioelectron 101:146–152
10. Deng YL, Xu DD, Pang DW, Tang HW (2017) Target-triggered signal turn-on detection of prostate specific antigen based on metal-enhanced fluorescence of Ag@SiO_2@SiO_2¯RuBpy composite nanoparticles. Nanotechnology 28:065501
11. Zhang GJ, Liu ZG, Fan LF, Guo YJ (2018) Electrochemical prostate specific antigen aptasensor based on hemin functionalized graphene-conjugated palladium nanocomposites. Microchim Acta 185:159
12. Deng SY, Lei JP, Liu Y, Huang Y, Ju HX (2013) A ferrocenyl-terminated dendrimer as an efficient quencher via electron and energy transfer for cathodic electrochemiluminescent bioanalysis. Chem Commun 49:2106–2108
13. Li XJ, Guo ZK, Li JX, Zhang Y, Ma HM, Pang XH, Du B, Wei Q (2015) Quenched electrochemiluminescence of Ag nanoparticles functionalized g-C_3N_4 by ferrocene for highly sensitive immunosensing. Anal Chim Acta 854:40–46
14. Lv YQ, Chen SY, Shen YF, Ji JJ, Zhou Q, Liu SQ, Zhang YJ (2018) Competitive multiple-mechanism-driven Electrochemiluminescent detection of 8-Hydroxy-2′-deoxyguanosine. J Am Chem Soc 140: 2801–2804
15. Zhu WJ, Khan MS, Cao W, Sun X, Ma HM, Zhang Y, Wei Q (2018) $Ni(OH)_2$ /NGQDs-based electrochemiluminescence immunosensor for prostate specific antigen detection by coupling resonance energy transfer with Fe_3O_4 @MnO_2 composites. Biosens Bioelectron 99:346–352
16. Qi HL, Li M, Dong MM, Ruan SP, Gao Q, Zhang CX (2014) Electrogenerated chemiluminescence peptide-based biosensor for the determination of prostate-specific antigen based on target-induced cleavage of peptide, anal. Chem 86:1372–1379
17. Zhang JJ, Jin R, Jiang DC, Chen HY (2019) Electrochemiluminescence-based capacitance microscopy for LabelFree imaging of antigens on the cellular plasma membrane. J Am Chem Soc 141:10294–10299
18. Gillan EG (2000) Synthesis of nitrogen-rich carbon nitride networks from an energetic molecular Azide precursor. Chem Mater 12:3906–3912
19. Shi YP, Lin H, Cui J, Qi HL, Liu ZJ, Cui GL (2013) The role of interleukin-17A in colorectal tumorigenesis. Cancer Biother Radio 28:429–432
20. Zhang KY, Lv SZ, Lin ZZ, Tang DP (2017) CdS:Mn quantum dot-functionalized g-C_3N_4 nanohybrids as signal-generation tags for photoelectrochemical immunoassay of prostate specific antigen coupling DNAzyme concatamer with enzymatic biocatalytic precipitation, Biosens. Bioelectron 95:34–40
21. Liu J, Wang HQ, Antonietti M (2016) Graphitic carbon nitride "reloaded": emerging applications beyond (photo)catalysis. Chem Soc Rev 45:2308–2326
22. Feng QM, Shen YZ, Li MX, Zhang ZL, Zhao W, Xu JJ, Chen HY (2016) Dual-wavelength electrochemiluminescence ratiometry based on resonance energy transfer between Au nanoparticles functionalized g-C_3N_4 Nanosheet and $Ru(bpy)_3^{2+}$ for microRNA detection. Anal Chem 88:937–944
23. Guo ZY, Wu L, Hu YF, Wang S, Li X (2017) Potential-resolved "in-electrode" type electrochemiluminescence immunoassay based on functionalized g-C_3N_4 nanosheet and Ru-NH_2 for simultaneous determination of dual targets. Biosens Bioelectron 95:27–33
24. Tian JQ, Liu Q, Asiri AM, Sun XP (2013) Ultrathin graphitic carbon nitride nanosheet: a highly efficient fluorosensor for rapid, ultrasensitive detection of Cu^{2+}. Anal Chem 85:5595–5599
25. Liu ZG, Xu M, Yang Z, Wang YX, Wang SQ, Wang HX (2017) Efficient removal of organic dyes from water by β-Cyclodextrin functionalized graphite carbon nitride composite. Chemistryselect. 2:1753–1758
26. Gao JW, Xiong HW, Zhang W, Wang Y, Wang HX, Wen W, Zhang XH, Wang SF (2018) Electrochemiluminescent aptasensor based on β-cyclodextrin/graphitic carbon nitride composite for highly selective and ultrasensitive assay of platelet derived growth factor BB. Carbon 130:416–423
27. Huo XL, Yang H, Li MX, Zhao W, Xu JJ, Wang Y, Luo XL, Chen HY (2018) Multi-segmented CdS–Au nanorods for electrochemiluminescence bioanalysis. Nanoscale 10:19224
28. Cao WD, Ferrance JP, Demas J, Landers JP (2006) Quenching of the electrochemiluminescence of tris(2,2′-bipyridine)ruthenium(II) by ferrocene and its potential application to quantitative DNA detection. J Am Chem Soc 128:7572–7578
29. Wang MD, Mao ZF, Kang TS, Wong CY, Mergny JL, Leung CH, Ma DL (2016) Conjugating a groove-binding motif to an Ir(III) complex for the enhancement of G-quadruplex probe behavior. Chem Sci 7:2516–2523
30. Wu C, Wu KJ, Liu JB, Zhou XM, Leung CH, Ma DL (2019) A dual-functional molecular strategy for in situ suppressing and visualizing of neuraminidase in aqueous solution using iridium(III) complexes. Chem Commun 55:6353–6356
31. Liu XP, Chen JS, Mao CJ, Niu HL, Song JM, Jin BK (2018) A label-free photoelectrochemical biosensor for urokinase-type plasminogen activator detection based on a g-C_3N_4/CdS nanocomposite. Anal Chim Acta 1025:99–107
32. Li PP, Cao Y, Mao CJ, Jin BK, Zhu JJ (2019) TiO_2/g-C_3N_4/CdS nanocomposite-based photoelectrochemical biosensor for ultrasensitive evaluation of T4 polynucleotide kinase activity. Ananl Chem 91:1563–1570
33. Maity P, Debnath T, Chopra U, Ghosh HN (2015) Cascading electron and hole transfer dynamics in a CdS/CdTe core-shell sensitized

with bromo-pyrogallol red (Br-PGR): slow charge recombination in type II regime. Nanoscale 7:2698–2707

34. Sha HF, Zhang Y, Wang YF, Ke H, Xiong X, Jia NQ (2019) Electrochemiluminescence resonance energy transfer biosensor between the glucose functionalized MnO_2 and g-C_3N_4 nanocomposites for ultrasensitive detection of concanavalin A. Biosens Bioelectron 124-125:59–65